NANO LETTERS

2007
Vol. 7, No. 7
2116−2121

Resonant Raman Spectroscopy of Individual Strained Single-Wall Carbon Nanotubes

Xiaojie Duan,[†,‡] Hyungbin Son,[†,§] Bo Gao,[‡] Jin Zhang,[*,‡] Tianjiao Wu,[‡] Georgy G. Samsonidze,[⊥] Mildred S. Dresselhaus,[§,||] Zhongfan Liu,[*,‡] and Jing Kong[*,§]

Centre for Nanoscale Science and Technology (CNST), Beijing National Laboratory for Molecular Sciences (BNLMS), Key Laboratory for the Physics and Chemistry of Nanodevices, State Key Laboratory for Structural Chemistry of Unstable and Stable Species, College of Chemistry and Molecular Engineering, Peking University, Beijing 100871, P. R. China, Department of Electrical Engineering and Computer Science and Department of Physics, Massachusetts Institute of Technology, Cambridge, Massachusetts 02139, and Department of Physics, University of California at Berkeley, Berkeley, California 94720

Received May 12, 2007; Revised Manuscript Received June 4, 2007

ABSTRACT

Resonance Raman spectra of individual strained ultralong single-wall carbon nanotubes (SWNTs) are studied. Torsional and uniaxial strains are introduced by atomic force microscopy manipulation. Torsional strain strongly affects the Raman spectra, inducing a large downshift in the E_2 symmetry mode in the G^+ band, but a slight upshift for the rest of the G modes and also an upshift in the radial breathing mode (RBM). Whereas uniaxial strain has no effect on the frequency of either the E_2 symmetry mode in the G^+ band or the RBM, it downshifts the rest of the G modes. The Raman intensity change reflects the effect of these strains on the SWNT electronic band structure.

Resonance Raman spectroscopy of single-wall carbon nanotubes (SWNTs) under strain[1−4] has attracted much attention during the past several years. The Raman intensity change can provide information on the electronic band structure of strained SWNTs,[5] which has important implications for the application of SWNTs to nanoelectromechanical systems (NEMS). Meanwhile, investigation of the response of different Raman modes to strain is also important to explore their physical origin, symmetry, and dependence on tube geometry.[6] In previous reports, due to the difficulty in controlling the deformation of SWNTs, some types of strain, such as torsion, were involved in a very limited way in the experiments. Furthermore, the use of SWNT ensembles with different chiralities and diameters often adds to the difficulty in identifying the intrinsic behavior of Raman modes under strain. For example, the expected different responses to strain of different high-energy tangential modes (G-band),[6] which correspond to distinct atomic displacement patterns, have not been reported so far.

In the present work, resonance Raman spectra of individual ultralong SWNTs under torsional and uniaxial strain induced by atomic force microscopy (AFM) manipulation have been investigated. It is found that the SWNT radial breathing mode (RBM) and G-band spectra respond differently to the two types of strains. Under torsional strain, the RBM frequency (ω_{RBM}) is found to upshift, and the G-band is found to split into multiple sub-bands in some cases, presumably due to the broken symmetry induced by torsion. The highest frequency mode in the G^+ band, which occurs around ∼1600 cm^{-1} and was assigned to the E_2 symmetry mode ($\omega_{E2G}{}^+$), downshifts significantly under torsional strain, whereas the other observed G modes slightly upshift. Under uniaxial strain, ω_{RBM} and $\omega_{E2G}{}^+$ do not have a noticeable response. In contrast, the other observed G modes are downshifted. Finally, the Raman intensity changes indicate that strain

* Corresponding authors. E-mail: jinzhang@pku.edu.cn (J.Z.). Telephone and Fax: 86-10-6275-7157. Prof. Jin Zhang, Center for Nanoscale Science and Technology (CNST), College of Chemistry & Molecular Engineering, Peking University, Beijing 100871, P. R. China.

† These authors have contributed equally to this work.

‡ Centre for Nanoscale Science and Technology (CNST), Beijing National Laboratory for Molecular Sciences (BNLMS), Key Laboratory for the Physics and Chemistry of Nanodevices, State Key Laboratory for Structural Chemistry of Unstable and Stable Species, College of Chemistry and Molecular Engineering, Peking University.

§ Department of Electrical Engineering and Computer Science, Massachusetts Institute of Technology.

|| Department of Physics, Massachusetts Institute of Technology.

⊥ Department of Physics, University of California at Berkeley.

10.1021/nl0711155 CCC: $37.00
Published on Web 06/14/2007

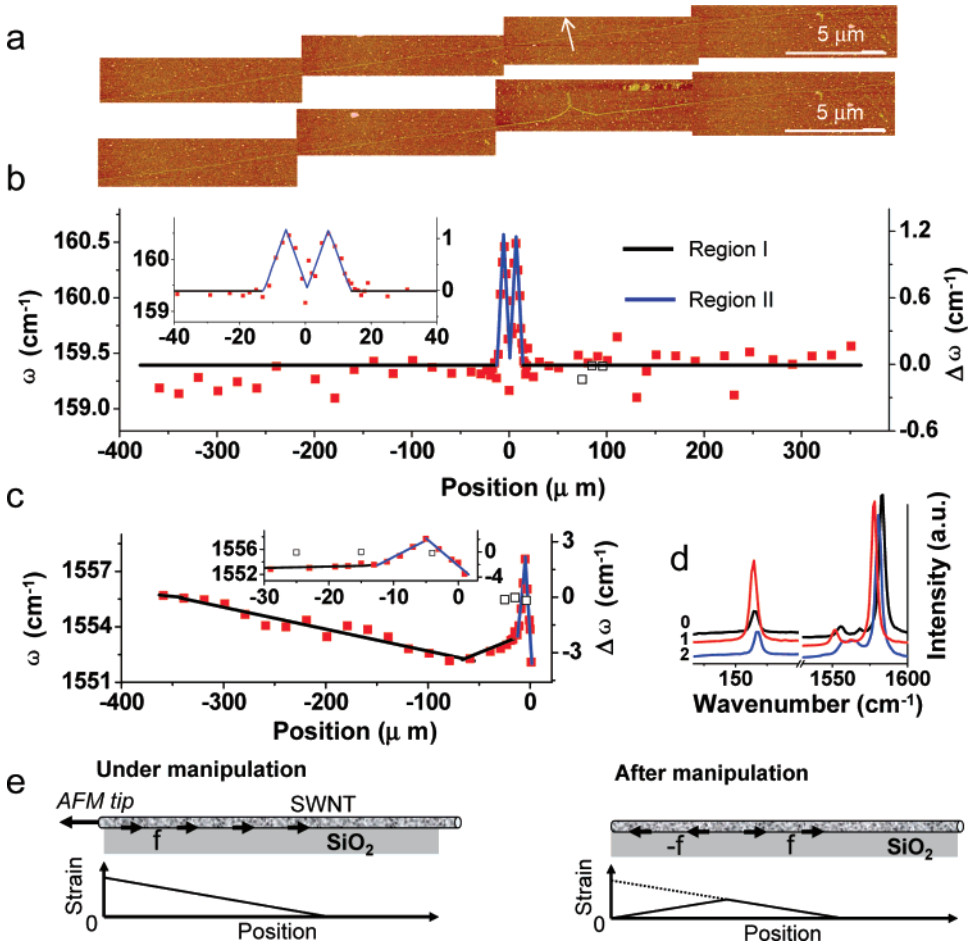

Figure 1. (a) Typical AFM images of a SWNT before (upper) and after (below) manipulation. The arrow is the tip path during manipulation. (b) and (c) are ω_{RBM} and ω_{G^-} profiles vs the position on SWNT no. 1. Open black and filled red squares are the frequencies before and after manipulation (same for following figures). The lines are the linear fit of the frequency distribution that reflects the strain distribution. Insets are enlarged frequency profiles. Panel (d) shows typical Raman spectra before (0) and after manipulation (1, 2). Spectra 1 and 2 are taken, respectively, at -59 and -5 μm. (e) Strain profiles vs position when the force is applied (left) and removed (right). Position 0 is the manipulation point.

perturbs the electronic band structure and therefore also perturbs the resonance Raman condition of SWNTs.

The SWNTs were grown on a silicon substrate with a 1 μm thick oxide layer using an ethanol chemical vapor deposition growth method, and the SWNTs typically had a length of several millimeters. All the SWNTs were straight and were oriented by the gas flow.[7] The AFM manipulation[8] was performed along a predefined path nearly perpendicular to the SWNT axis at a point millimeters away from the two ends. Figure 1a shows typical AFM images of a SWNT before and after manipulation, whereby the SWNT was dragged out by about 3−4 μm around the manipulation point. There is no morphological change at other positions along the SWNT axis. All SWNTs in this paper have been manipulated repeatedly in this way, and none of them were split into multiple nanotubes as a result of the manipulations. Because it is very common for a SWNT bundle to split up into multiple tubes under AFM manipulations, we believe that all the nanotubes investigated in this work are individual SWNTs rather than bundles of nanotubes.

The resonant micro-Raman spectra were collected along the SWNT axis using a 632.8 nm He−Ne laser. The laser polarization was parallel to the tube axis. The excitation spot size was about 1−2 μm and the laser power was 8 mW/μm^2.[9] All the Raman features were fitted to Lorentzian line shapes to obtain the peak frequency and intensity. Parts b and c of Figure 1 show the frequency profiles versus the position on SWNT no. 1 after AFM manipulation. The manipulation point is at position 0, and two regions are defined along the nanotube: the region from -12 to 12 μm is defined as region II, and the regions from 12 to 350 μm and from -350 to -12 μm are defined as region I. Very different responses of the RBM and G-band spectra were observed in these two regions. The Raman spectra before manipulation and the spectra collected at -59 μm (region I) and -5 μm (region II) after manipulation are shown in Figure 1d. This SWNT has an RBM peak at 159.4 cm^{-1} (Figure 1b), and the G$^-$ peak is at 1555.6 cm^{-1}(Figure 1c) originally. After manipulation, in region I, it can be seen that ω_{RBM} does not shift compared to its original value (Figure 1b), whereas ω_{G^-} downshifts along the SWNT (from -12 to -59 μm) and then slowly approaches back toward its unperturbed value from -59 to -350 μm (Figure 1c), giving rise to a "V" shaped ω_{G^-} response along the SWNT

in region I. On the other hand, in region II, both ω_{RBM} (Figure 1b) and ω_G^- (Figure 1c) upshift via a "Λ" shaped pattern along the SWNT. A close examination reveals that the "Λ" shaped upshift of ω_G^- in region II is added on top of the downshifted values extending from region I. These results indicate that the AFM manipulation has induced two different effects on the SWNT due to different physical mechanisms. Mechanism 1 has a much longer length scale (up to 350 μm in this case), which results in the downshift of ω_G^-, but has no influence on ω_{RBM}. Mechanism 2 has a smaller length scale (~10 μm), which upshifts both ω_{RBM} and ω_G^-, as shown in the experimental data.

The factors that may influence the SWNT Raman spectra include temperature,[10] charge transfer,[11] the interaction between the tube and the substrate,[12] and the SWNT deformations. In our experiment, because the nanotubes remain on the same substrate, only the tube region within 3−4 μm of the AFM manipulation points (see Figure 1a) are being perturbed, and there is no temperature variation along the SWNT. Clearly the substrate interactions, temperature, or charge transfer are not the reasons for the aforementioned Raman spectra variation along the SWNT. The possible deformations of the nanotubes from the AFM manipulation include tube bending, buckling or radial squashing under the AFM tip, uniaxial expansion or compression, or torsional twist. From the AFM image in Figure 1a, we see that the SWNT is bent in a region of 3−4 μm, which is inconsistent with the length scale of the observed "V" or "Λ" patterns in regions I and II in Figure 1, and therefore the bending by itself cannot be the reason for the much longer range of the changes observed in the Raman spectra. Similarly, the possible radial compression caused by AFM tip dragging and pressing on the SWNT would also occur on a much smaller length scale than regions I and II and thus can also be excluded as the driving mechanism.

We therefore conclude that the only possibilities left are uniaxial and torsional strains, which can propagate along the SWNTs. When the AFM tip drags a SWNT sideways, there will be a simultaneous rolling and sliding movement of the SWNT, giving rise to both a torsional twist and an axial elongation in the SWNT. It has been previously reported that uniaxial strain does not influence ω_{RBM} but downshifts ω_G,[1] which has also been shown by our study of SWNTs subjected to pure uniaxial strain when grown on trenched substrates.[13] These prior works are consistent with our present result, which indicates that uniaxial strain is the dominant mechanism for the observed changes in the Raman spectra observed in region I. This leaves the torsional twist to be the dominant mechanism for the ω_{RBM} and ω_G upshifts in region II of Figure 1. Because the torsional deformation occurs normal to the tube axis, it is reasonable that the phonon modes that either have vibrations (such as the RBM or the TO modes in the G-band) or symmetry effects in the directions normal to the tube axis (such as the E_1 and E_2 symmetry modes in the G-band) will be affected. More evidence confirming the existence of torsional strain will be presented in the following data. The formation of torsional strain supports the picture of a SWNT rolling under AFM manipulation. Similar rolling phenomena have been observed during AFM manipulation of CNTs on HOPG.[14]

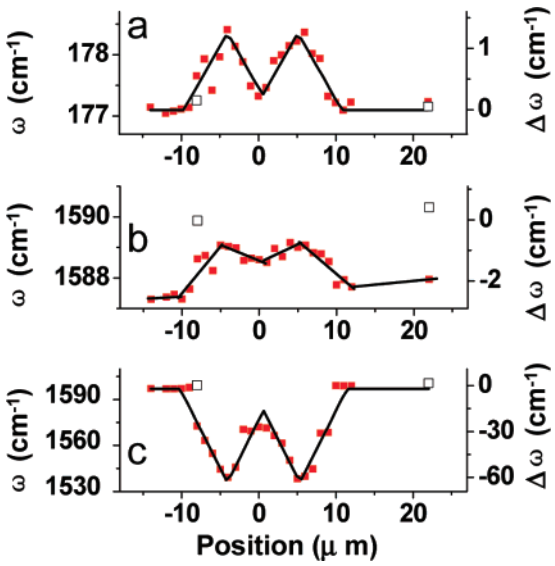

Figure 2. Frequency profiles vs position along SWNT no. 2. Open (black) and filled (red) squares denote the frequencies before and after manipulation. The Raman peaks are originally at 177.1 cm^{-1} (a), 1589.9 cm^{-1} (b), and 1599.1 cm^{-1} (c).

The profiles of the frequency shifts due to the uniaxial and torsional strains reflect the propagation of these two types of strains along the SWNT. As shown in Figure 1e, under the AFM manipulation, the strain decreases along the tube axis starting from the manipulation point because of the substrate friction that acts on the movement of the SWNTs. If the friction is constant, the decrease will be linear. After the tip is removed, the elastic retraction of the nanotubes in combination with the friction will result in a triangular strain profile, as shown in the right panel of Figure 1e, giving rise to the "Λ" and "V" shaped frequency shift profiles. Because these profiles occur on both sides of the manipulation point, a pattern of "M" or "W" will be generated. In general, uniaxial strain is found to propagate to a longer length scale (up to 350 μm in SWNT no. 1) than torsional strains (~12 μm in SWNT no. 1), and region II (between −12 and 12 μm) is the region over which both uniaxial and torsional strain exist.

In our study, we found that, for ω_{RBM}, torsion always gives rise to a frequency upshift and uniaxial strain has no influence, whereas for the G-band, different component modes with different symmetries have different responses to torsional and uniaixal strains. This can be seen in Figure 2 from SWNT no. 2 with RBM at 177.1 cm^{-1} before manipulation. The propagation range of the torsional strain in this tube is indicated by the ω_{RBM} profile from −10 to 12 μm in Figure 2a. In this region, the frequency of the mode originally at 1589.9 cm^{-1} in the G^+ band shows an "M" shaped profile (Figure 2b), corresponding to an upshift under the torsional strain followed by an accompanying relaxation. However, the frequency profile of the peak originally at 1599.1 cm^{-1} has a shape of "W" (Figure 2c), suggesting its downshift by torsional strain. It should be noted that the downshift of this peak (maximum: ~60 cm^{-1}) is much larger

Table 1. Frequency Shift Results for Different Modes of Different SWNTs under Torsional and Uniaxial Strain[a]

Type	diameter d (nm)	ω_{RBM} (cm^{-1})	ω_{G1} (cm^{-1})	ω_{G2} (cm^{-1})	ω_{G3} (cm^{-1})	ω_{G4} (cm^{-1})	ω_{G5} (cm^{-1})
	1.88	127.8 +	1600.0 - (-77.9)	1592.0 +	1576.5 +		
	1.61	148.5 +		1591.8 +	1576.6 +	1566.1 +	
S	1.53	155.9 +	1599.4 - (<-18.6)	1584.6 +	1569.6 +		1557.3 +
	1.49	159.4 +		1582.7 +	1568.0 +		1555.6 +
	1.48	160.6 +	1601.0 - (<-8.2)	1586.8 +	1570.8 +	1564.0 +	
	1.37	177.1 +	1599.1 - (-57.7)	1589.9 + (1.5)	1576.5 - (-21.5)		
	1.29	187.1 +		1584.6 +			
	1.24	195.5 +		1593.4 +	1580.5 +	1563.4+	1559.0 - (-4.9)
M	1.21	198.9 +	1598.6 - (-26.2)	1582.5 - (-33.3)			1558.5 - (-25.2)
	1.16	207.8 +	1601.0 - (-44.7)				
	1.13	211.9 +	1593.6 - (-89.9)	1588.8 +			
	1.10	218.6 +	1592.1 - (-49.9)	1586.1 - (-39.8)			

[a] The values listed are the original frequencies before manipulation. For some of the peaks, the maximum frequency shift is also listed in parenthesis. The "<" in the parenthesis is due to the fact that the Raman signal is too weak to be observed at maximum frequency shift point, therefore, values close to the maximum frequency shift is being reported. Type *S* or *M* means the SWNT is semiconducting or metallic. Although there are six modes in the G-band, in our studies, we only observed five Peaks. They are labeled G1, G2, ... based on the frequency values, and this notation has no other meaning. The diameters are from equation $\omega_{RBM} = A/d + B + (C + D\cos^2 3\theta)/d^2$.[19] The second-order terms *C* and *D* was not included here: $A = 227$ cm^{-1} nm; for semiconducting SWNTs: $B = 7.3$ cm^{-1}; for metallic SWNTs: $B = 11.8$ cm^{-1}.

than the upshift of the peak at 1589.9 cm^{-1} (maximum: 1.5 cm^{-1}), suggesting its high sensitivity to torsion. From Figure 2b, it can be also seen that, although the M shaped profile indicates an upshift, there is an overall downshift compared to the original 1589.9 cm^{-1} frequency due to the coexistence of uniaxial strain. Another important characteristic is that, although uniaxial strain propagates farther than the torsional strain, as reflected by the frequency shift in Figure 2b, the peak at 1599.1 cm^{-1} has recovered to its original frequency even in the presence of uniaxial strain. This indicates that this mode (1599.1 cm^{-1}) is not sensitive to the uniaxial strain, which is different from other G modes commonly reported.[1,2]

Table 1 lists the frequency shift results of twelve SWNTs, including five semiconducting and seven metallic tubes.[15] "+" and "−" represents an upshift and a downshift, respectively, caused by torsion. The original peak frequencies are listed and the maximum shift numbers are indicated for some peaks in parentheses. Red color means the corresponding G mode downshifts under uniaxial strain, while blue means it does not shift. Several important facts can be noticed from this summary directly: First, it can be seen that all ω_{RBM} were upshifted by torsional strain and were not affected by uniaxial strain. Second, in this table, the peaks in the G-band are grouped based on their frequency values, therefore for different nanotubes, the same ω_{Gi} ($i = 2, ..., 5$) can belong to different symmetry modes, but ω_{G1} is an exception, and we have observed very consistent responses for ω_{G1} in all nanotubes. This mode is always largely downshifted by torsional strain (the downshift can be as large as 90 cm^{-1}), but is not sensitive to uniaxial strain. We believe this mode should correspond to the E_2 symmetry mode of the G^+ band.[16] In addition, the other observed G modes in semiconducting nanotubes downshift with uniaxial strain (consistent with previous results[1,13]) and slightly upshift with torsional strain. The behaviors of the other G modes in metallic nanotubes appear to be complicated, and we do not have a clear understanding at this stage. It should also be noted that, although there are six G-band modes for nanotubes (*A*, E_1, E_2 symmetry for both LO and TO modes[16]), not every mode has been seen in our experiments. Another interesting phenomenon is that all G modes with a "+" are red while all "−" are blue. This means that the G modes that were downshifted by torsional strain had no change under uniaxial strain, and the G modes that were upshifted by torsion always downshift under uniaxial strain. In general, under torsion, the magnitude of the downshift was much larger than that of the upshift (tens of cm^{-1} for the downshift and a few cm^{-1} for the upshift).

The Raman frequency shifts can be understood on the basis of C−C bonds length changes. Torsional strain will mainly cause the C−C bonds to stretch or compress in the circumferential direction, whereas uniaxial strain corresponds to the stretch or compression in the axial direction. Thus the Raman modes corresponding to the vibration with an atomic displacement pattern mainly in the circumferential or radial direction will be most sensitive to the torsional strain and the modes vibrating in the axial direction will be most sensitive to the uniaxial strain, respectively. This is consistent with the result that ω_{RBM} and the $\omega_{E2G}{}^+$ mode are sensitive to torsional strain, while insensitive to uniaxial strain, and

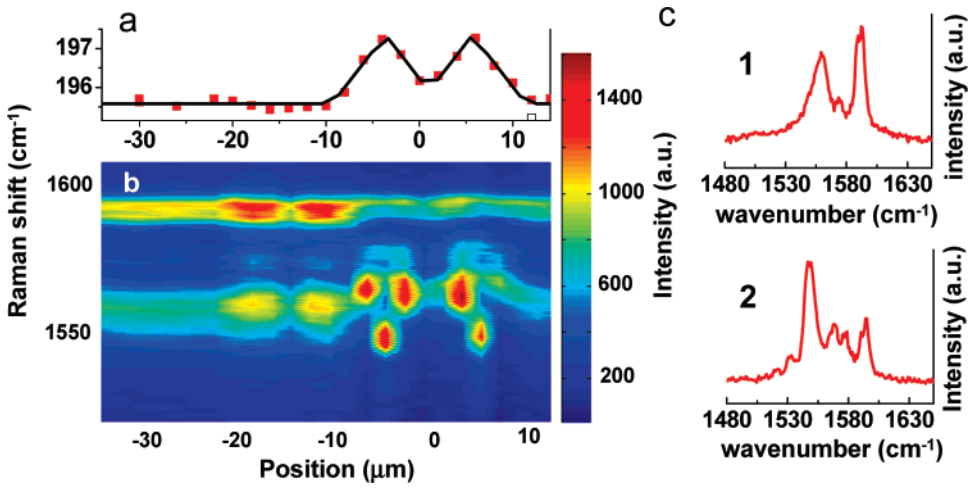

Figure 3. (a) ω_{RBM} (cm^{-1}) profile vs position (μm). (b) G-band spectra mapping image vs position along the SWNT with ω_{RBM} at 195.5 cm^{-1}. (c) G-band spectra from positions (1) and (2) without torsion and with maximum torsion, respectively.

other G modes have higher sensitivity to uniaxial than torsional strain. It has been calculated that torsional strain will cause some C−C bonds to stretch and some others to compress.[4] Therefore, it is understandable that a downshift and an upshift can occur for different G modes with different symmetries under torsional strain. However, under uniaxial stretch, only a downshift is observed for certain G modes due to the elongation of C−C bonds in the axial direction.

Because torsion can cause symmetry breaking, it was predicted that torsion will induce mode splitting in the Raman G-band spectra.[4] We have also observed this phenomenon in our data. Seen in Figure 3c are Raman G-band spectra from two positions without torsion (spectrum 1) and with maximum torsion (spectrum 2). Spectrum 2 contains more peaks than spectrum 1. It appears that the new peaks originate from the splitting of the low-frequency peak around 1559.0 cm^{-1} in spectrum 1. The degeneracy for phonon vibrations with right- and left-handed displacements before manipulations could be broken as a result of the broken symmetry due to torsional strain.[4]

Strain can also change the Raman peak intensity, which reflects the effect of the strain on the SWNT electronic band structure. From resonance Raman theory, given the value of the line width Γ, the electronic transition energy E_{ii} can be estimated from the anti-Stokes to Stokes intensity ratio I_{AS}/I_S[17]

$$\frac{I_{AS}}{I_S} = \frac{|(E_{laser} - E_{ii} - i\Gamma)(E_{laser} - E_{ph} - E_{ii} - i\Gamma)|^2}{|(E_{laser} - E_{ii} - i\Gamma)(E_{laser} + E_{ph} - E_{ii} - i\Gamma)|^2} \exp\left(-\frac{E_{ph}}{k_B T}\right) \quad (1)$$

Here, E_{laser} and E_{ph} are the energy of the incident laser and the phonon energy, respectively. The last exponential term is the Bose−Einstein thermal factor, in which k_B is the Boltzmann constant and T is the temperature.

Figure 4 gives the results for the electronic transition energies E_{ii} of the above SWNT no. 1 as a function of position along the tube. Here, E_{laser} is 1.959 eV (632.8 nm). One can see from the Kataura plot that this E_{laser} value corresponds to resonance with the E_{33} transition.[7] For this tube, setting Γ as 35 meV gives the best fit between the

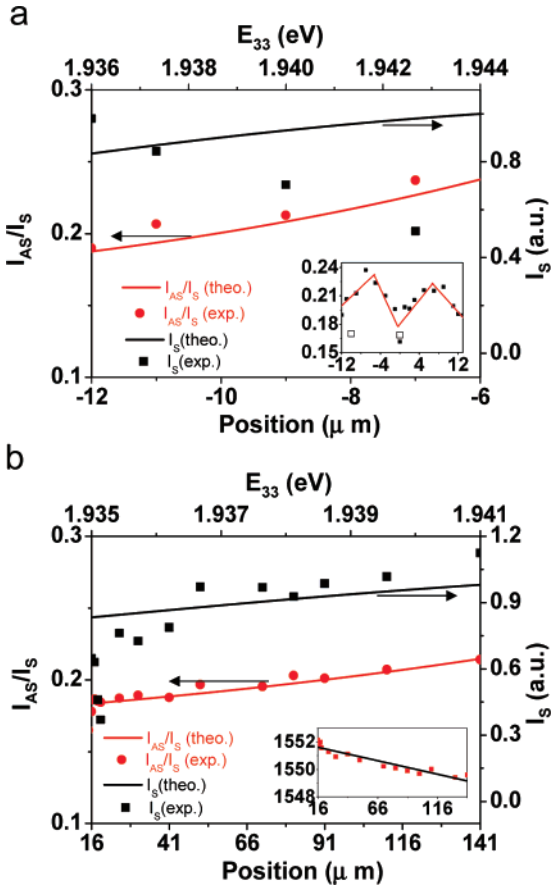

Figure 4. E_{33} calculation results for SWNT no. 1 under torsional (a) and uniaxial strain (b). The red circles and black squares are the experimental I_{AS}/I_S and I_S at different positions, as shown on the bottom axes. The red and black lines are the calculated I_{AS}/I_S and I_S corresponding to different E_{33} as shown on the top axes. Inset in (a) is the I_{AS}/I_S profile vs position (μm) in the torsion region. The open squares indicate the value before AFM manipulation. Inset in (b) is the corresponding ω_G^- (cm^{-1}) profile (originally at 1555.6 cm^{-1}) vs position (μm).

experimental and theoretical I_S and I_{AS}/I_S, and therefore $\Gamma = 35$ meV has been used for the following calculation. From the initial I_{AS}/I_S before manipulation, the calculation yields a value of 1.930 eV for the E_{33} optical transition energy before AFM manipulation of the tube. As seen in the inset of Figure 4a, the I_{AS}/I_S ratio also shows an M-shaped distribution which is closely correlated with ω_{RBM} over the whole torsional strain region. By calculating E_{33} from I_{AS}/I_S along SWNT no. 1 with eq 1, an increase in the ratio I_{AS}/I_S is found in the region from -12 to -6 μm, where the torsional strain increased linearly from zero to the maximum value, corresponding to an increase of E_{33} from 1.936 to 1.944 eV. In this short distance region, although uniaxial strain also exists, the effect of uniaxial strain on E_{33} is negligible in comparison to that of the torsional strain. Assuming that uniaxial strain causes a linear change in E_{33}, the E_{33} change due to uniaxial strain in this region would be less than 0.3 meV as calculated from the results in Figure 4b, which is much less than the 8 meV energy change due to torsional strain. Thus the increase of E_{33} in region II can be almost entirely attributed to torsion. The same analysis in the region from 16 to 141 μm is shown in Figure 4b. In this region, only uniaxial strain exists and causes an increase in E_{33} from 1.935 to 1.941 eV. Thus, for this tube, both torsional and uniaxial strain cause E_{33} to increase, but by very different amounts. As can be seen from Figure 4a and b, the calculated I_{AS}/I_S and I_S curves fit the experimental data very well except for the variation of I_S along the SWNT inside the torsional region. This deviation indicates a dependence on torsion of the electron−phonon coupling matrix element of the RBM signal intensity. This SWNT no. 1 may be assigned to be (13,9).[7] The torsional and uniaxial strain dependences of the SWNT electronic band structure are consistent with theoretical predictions.[18] The direction and magnitude of these strain effects also depend on the (n,m) of the SWNTs.

In summary, using AFM manipulation on individual ultralong SWNTs, different effects on the Raman spectra of SWNTs are observed for torsional strain as compared to uniaxial strain and these different responses involve different vibrational modes with different symmetries for each type of strain. The resonance Raman intensity variation is shown to reflect the effect of torsional and uniaxial strains on the E_{ii} transition energies. Significant difference of the different modes in response to strain can also provide valuable information for studying their origin, symmetry, and dependence on tube geometry, which is important for the development of the theoretical framework for this aspect of SWNT Raman spectroscopy.

Acknowledgment. This work was supported by NSFC (20573002, 20673004, 50521201) and MOST (2006CB932701, 2006CB932403). H. Son and J. Kong gratefully acknowledge support from the Intel Higher Education Program. M. S. Dresselhaus acknowledges support from NSF DMR 04-05538.

References

(1) Cronin, S. B.; Swan, A. K.; Unlu, M. S.; Goldberg, B. B.; Dresselhaus, M. S.; Tinkham, M. *Phys. Rev. Lett.* **2004**, *93*, 167401.
(2) Cronin, S. B.; Swan, A. K.; Unlu, M. S.; Goldberg, B. B.; Dresselhaus, M. S.; Tinkham, M. *Phys. Rev. B* **2005**, *72*, 035425.
(3) Venkateswaran, U. D.; Brandsen, E. A.; Schlecht, U.; Rao, A. M.; Richter, E.; Loa, I.; Syassen, K.; Eklund, P. C. *Phys. Status Solidi B* **2001**, *223*, 225.
(4) Wu, G.; Zhou, J.; Dong, J. M. *Phys. Rev. B* **2005**, *72*, 115411.
(5) Souza, A. G.; Kobayashi, N.; Jiang, J.; Gruneis, A.; Saito, R.; Cronin, S. B.; Mendes, J.; Samsonidze, G. G.; Dresselhaus, G. G.; Dresselhaus, M. S. *Phys. Rev. Lett.* **2005**, *95*, 217403.
(6) Reich, S.; Thomsen, C.; Ordejon, P. *Phys. Rev. B* **2001**, *64*, 195416.
(7) Zhang, Y. Y.; Zhang, J.; Son, H. B.; Kong, J.; Liu, Z. F. *J. Am. Chem. Soc.* **2005**, *127*, 17156.
(8) Duan, X. J.; Zhang, J.; Ling, X.; Liu, Z. F. *J. Am. Chem. Soc.* **2005**, *127*, 8268.
(9) Similar result were obtained under lower laser power, such as 1.07 and 0.043 mW, therefore the laser heating effect is excluded.
(10) Zhou, Z. P.; Dou, X. Y.; Ci, L. J.; Song, L.; Liu, D. F.; Gao, Y.; Wang, J. X.; Liu, L. F.; Zhou, W. Y.; Xie, S. S.; Wan, D. Y. *J. Phys. Chem. B* **2006**, *110*, 1206.
(11) Okazaki, K.; Nakato, Y.; Murakoshi, K. *Surf. Sci.* **2004**, *566*, 436.
(12) Zhang, Y. Y.; Son, H. B.; Zhang, J.; Dresselhaus, M. S.; Kong, J.; Liu, Z. F. *J. Phys. Chem. C* **2007**, *111*, 1983.
(13) Son, H. B. et al., *Appl. Phys. Lett.*, submitted
(14) Falvo, M. R.; Taylor, R. M.; Helser, A.; Chi, V.; Brooks, F. P.; Washburn, S.; Superfine, R. *Nature* **1999**, *397*, 236.
(15) Jorio, A.; Saito, R.; Hafner, J. H.; Lieber, C. M.; Hunter, M.; McClure, T.; Dresselhaus, G.; Dresselhaus, M. S. *Phys. Rev. Lett.* **2001**, *86*, 1118.
(16) Jorio, A.; Dresselhaus, G.; Dresselhaus, M. S.; Souza, M.; Dantas, M. S. S.; Pimenta, M. A.; Rao, A. M.; Saito, R.; Liu, C.; Cheng, H. M. *Phys. Rev. Lett.* **2000**, *85*, 2617.
(17) Souza, A. G.; Jorio, A.; Hafner, J. H.; Lieber, C. M.; Saito, R.; Pimenta, M. A.; Dresselhaus, G.; Dresselhaus, M. S. *Phys. Rev. B* **2001**, *63*, 241404.
(18) Yang, L.; Han, J. *Phys. Rev. Lett.* **2000**, *85*, 154.
(19) Jorio, A.; Fantini, C.; Pimenta, M. A.; Capaz, R. B.; Samsonidze, G. G.; Dresselhaus, G.; Dresselhaus, M. S.; Jiang, J.; Kobayashi, N.; Gruneis, A.; Saito, R. *Phys. Rev. B* **2005**, *71*, 075401.

NL0711155